Article

The origin of placental mammal life histories

https://doi.org/10.1038/s41586-022-05150-w

Received: 15 October 2021

Accepted: 27 July 2022

Published online: 31 August 2022

Check for updates

Gregory F. Funston[1,5]✉, Paige E. dePolo[1], Jakub T. Sliwinski[2], Matthew Dumont[2], Sarah L. Shelley[1], Laetitia E. Pichevin[1], Nicola J. Cayzer[1], John R. Wible[3], Thomas E. Williamson[4], James W. B. Rae[2] & Stephen L. Brusatte[1]✉

After the end-Cretaceous extinction, placental mammals quickly diversified[1], occupied key ecological niches[2,3] and increased in size[4,5], but this last was not true of other therians[6]. The uniquely extended gestation of placental young[7] may have factored into their success and size increase[8], but reproduction style in early placentals remains unknown. Here we present the earliest record of a placental life history using palaeohistology and geochemistry, in a 62 million-year-old pantodont, the clade including the first mammals to achieve truly large body sizes. We extend the application of dental trace element mapping[9,10] by 60 million years, identifying chemical markers of birth and weaning, and calibrate these to a daily record of growth in the dentition. A long gestation (approximately 7 months), rapid dental development and short suckling interval (approximately 30–75 days) show that *Pantolambda bathmodon* was highly precocial, unlike non-placental mammals and known Mesozoic precursors. These results demonstrate that *P. bathmodon* reproduced like a placental and lived at a fast pace for its body size. Assuming that *P. bathmodon* reflects close placental relatives, our findings suggest that the ability to produce well-developed, precocial young was established early in placental evolution, and that larger neonate sizes were a possible mechanism for rapid size increase in early placentals.

Placentals are the most diverse group of mammals, comprising more than 6,000 extant species[11] and the largest animals ever. Their success may relate to their derived life history[8,12], with maternal investment shifted prenatally through extended gestation[7,13]. This adaptation allows placentals the unique capability among mammals to produce highly precocial young: typically single offspring born at larger masses with well-developed dentition, fur and open eyes[13,14]. Extended gestation may have released placentals from developmental constraints associated with prolonged lactation in other mammals[8,15,16], enabling experimentation with new locomotor modes and habitats[17,18]. However, when extended gestation evolved in mammals remains unclear; Mesozoic eutherians (mammals more closely related to placentals than marsupials) did not grow like living placentals[19–21] and it has been hypothesized that ancestral placentals gave birth to altricial young[21]. Nonetheless, immediately after the end-Cretaceous extinction, early Palaeocene placentals emerged from a 100 million years ago (Ma) lineage of small-bodied ancestors and quickly achieved much greater masses as they diversified into various niches[4]. Thus, the early Palaeocene was probably an important interval in the eutherian transition to placental-like growth strategies, but the life histories of these mammals remain unknown.

Among early placental clades, the Palaeocene–Eocene Pantodonta are a key group, because they were among the first large mammalian herbivores, becoming the largest mammals ever up to that point in time[22]. The early Palaeocene (approximately 62 Ma) *P. bathmodon* (approximately 42 kg) is represented by multiple skeletons representing most of its ontogeny, including a small juvenile with deciduous dentition and unfused epiphyses (New Mexico Museum of Natural History and Science (NMMNH) P-27844; approximately 17 kg at death). As one of the largest mammals in its ecosystem[23], its life history might provide insight into the relationship between life history and body size in Palaeocene eutherians.

Life histories of extinct animals can be reconstructed using incremental growth features of mineralized tissues such as bones and teeth[24–26]. Bones preserve evidence of stress and annual cycles[27,28], and they accurately reflect growth rate throughout life[29,30], including changes associated with maturity[31]. In teeth, daily incremental lines in the dentine and enamel allow for precise chronologies and faithful recording of life history events including birth and nutritional stress such as that experienced during weaning[32,33], whereas cementum preserves annual growth cycles[24,34]. Chemical signals of birth and early-life diet are recorded in the developing teeth by the abundances of certain trace elements, such as zinc (Zn), which is enriched at birth[35,36], and barium (Ba), which varies according to bioavailability in the diet[26]. When integrated with daily growth increments, trace element maps can reveal birth and the timing of weaning, a technique applied to primates up to 2.6 million years of age[9,10,26], but with unrealized potential in other fossil mammals.

Here we combine palaeohistological and geochemical evidence to reconstruct the life history of *P. bathmodon* on a daily scale and evaluate the physiology of a key group in the rise of mammals following the end-Cretaceous mass extinction. These data provide unprecedented insight into the life history of a fossil mammal, revealing that characteristic placental reproductive strategies were established early in their evolution.

[1]School of GeoSciences, University of Edinburgh, Edinburgh, UK. [2]School of Earth and Environmental Sciences, University of St Andrews, St Andrews, UK. [3]Carnegie Museum of Natural History, Pittsburgh, PA, USA. [4]New Mexico Museum of Natural History and Science, Albuquerque, NM, USA. [5]Present address: Department of Natural History, Royal Ontario Museum, Toronto, Ontario, Canada. ✉e-mail: Gregory.Funston@ed.ac.uk; Stephen.Brusatte@ed.ac.uk

Dental development, birth and weaning

Incremental growth features are well preserved in the teeth, especially the enamel, and are clearly visible in histological thin sections (Fig. 1b–g and Extended Data Fig. 1). Daily laminations in the dentine and enamel[37] (Fig. 1b,c,e) track the successive growth of the tooth crown (Extended Data Table 1). High-resolution trace element mapping of several teeth (Extended Data Table 1 and Supplementary Figs. 1–7) reveals patterns in Zn and Ba that correspond to these incremental growth patterns and provide evidence of birth and weaning in *P. bathmodon* (Fig. 2), extending the viable window for dietary trace element mapping by roughly 60 million years compared with previous studies[10]. The most complete record of early life comes from a second lower molar of an adult individual (NMMNH P-19541), in which both the neonatal event and the weaning transition are preserved (Fig. 2).

Birth is recorded in the enamel by a prominent neonatal line (Figs. 1g and 2b), a discontinuity in the enamel prisms reflecting developmental disruptions in response to the physiological stress of birth[38]. The neonatal line is Zn-enriched (Fig. 2b and Extended Data Fig. 2), as observed in modern teeth, in which this results from changing levels of Zn in serum over the birth interval and the ingestion of Zn-rich colostrum[35,36]. The neonatal line is Zn-enriched in multiple cusps of the tooth, and no other accentuated lines in the enamel of this or other teeth are Zn-enriched (Fig. 2b; see Supplementary Information). This suggests that analysis of Zn may be useful as an independent criterion for distinguishing neonatal lines from other accentuated lines in fossil mammals[36].

Concentrations of Ba in the enamel were elevated postnatally, but decrease sharply after a short period (Fig. 2c). This pattern is present in both the protoconid and the paraconid of the second lower molar, as well as in the first lower molar of the same individual (Fig. 2d), indicating

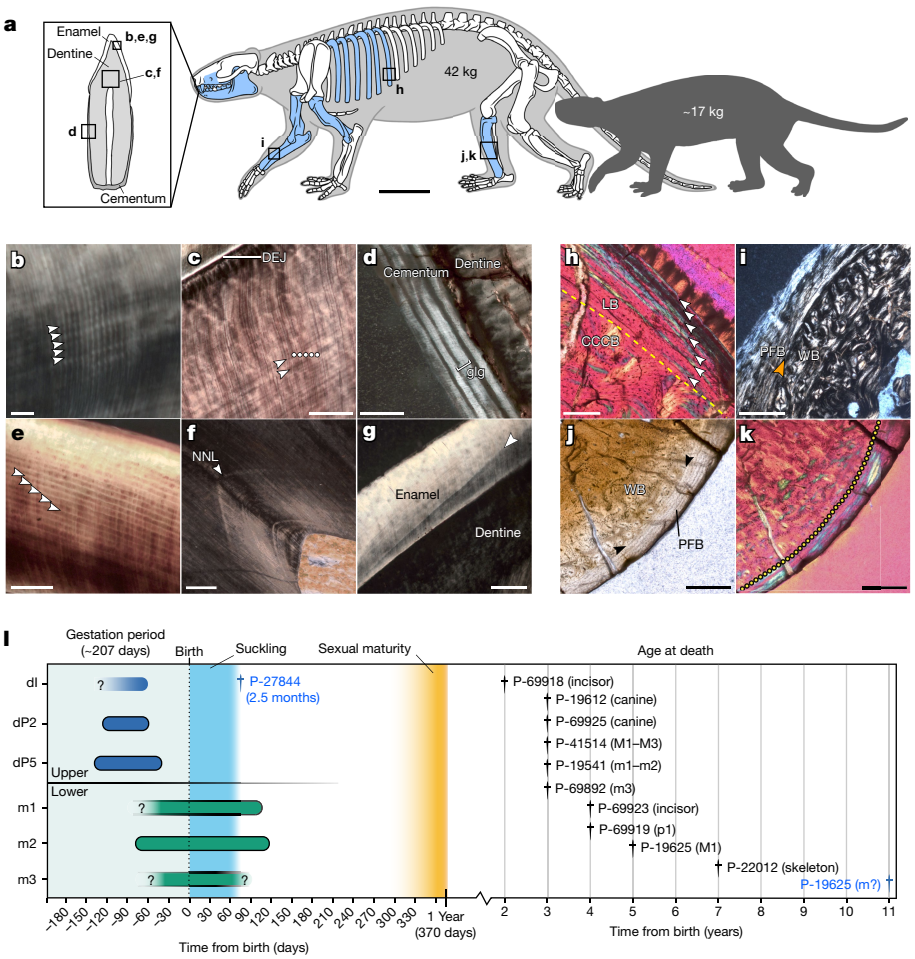

Fig. 1 | Palaeohistology of *P. bathmodon*. **a**, Skeletal reconstruction of adult, with sampled elements in blue. The boxes show the representative locations of palaeohistological images, and the silhouette shows the relative size of juvenile NMMNH P-27844. **b**–**g**, Dental features used for reconstruction of life history (all coronal sections): enamel cross-striations (arrowheads) in the second lower molar of NMMNH P-19541 (**b**); lines of von Ebner in the deciduous ultimate upper premolar of NMMNH P-27844 (the white dots mark five lines and the arrowheads show the orientation of the lines) (**c**); cementum annulations (one light and one dark band) in the first lower premolar of NMMNH P-69919 (**d**); daily laminations (arrowheads) in the lower incisor of NMMNH P-69918 (**e**); the neonatal line (NNL; arrowhead) in the dentine of the deciduous ultimate upper premolar of NMMNH P-27844 (**f**); and the NNL (arrowhead) in the enamel of the second lower molar of NMMNH P-19541 (**g**). **h**–**k**, Osteohistological features used for reconstruction of life history (all transverse midshaft diaphysis sections): the lines of arrested growth (arrowheads) in the outer cortex of the rib of NMMNH P-22012; dashed yellow line indicates boundary between compact coarse cancellous bone (CCCB) and primary lamellar bone (LB) (**h**); the annulus (orange arrowhead) at weaning transition in the radius of NMMNH P-27844 (**i**); weaning transition (arrowheads and yellow dotted line) in the outer cortex of the tibia of NMMNH P-27844 under plane polarized light (**j**) and cross-polarized light with a lambda filter (**k**). Images in **b**–**g**, **i** are under cross-polarized light, and the image in **h** is under cross-polarized light with a lambda filter. **l**, Life history chronology of *P. bathmodon* showing crown formation times for deciduous (blue) and adult (green) teeth, life history events and mortality. Daggers indicate ages at death; youngest and oldest specimens are in blue. Scale bars, 10 cm (**a**), 25 µm (**b**), 50 µm (**e**), 100 µm (**c**,**d**), 200 µm (**f**–**h**) and 500 µm (**i**–**k**). CCCB, compact coarse cancellous bone; DEJ, dentinoenamel junction; dI, deciduous incisor; dP2, deciduous upper second premolar; glg, growth layer group; LB, lamellar bone; m1, lower first molar; M1, upper first molar; PFB, parallel-fibred bone; p1, lower first premolar; WB, woven-fibred bone.

that it represents a consistent biogenic signal. Temporary postnatal Ba enrichment in *P. bathmodon* is identical to that reported in modern and fossil primates[9,10,26], in which it reflects the increased bioavailability of Ba in breastmilk[26]. The decreased levels in Ba presumably mark the onset of weaning and indicate a minimum suckling period of about 31–56 days in *P. bathmodon*. Further independent evidence for a short suckling period also comes from mesowear and microwear in the dentition of a young juvenile (NMMNH P-27844; Extended Data Fig. 3), where growth increments in the dentine of the deciduous teeth are exceptionally well preserved (Fig. 1c and Extended Data Fig. 1). Like in the enamel, a birth signature appears to be recorded in the dentine by a neonatal line, and in this individual, the postnatal dentine is Zn-enriched (Extended Data Fig. 4). Dentine continues to infill the pulp cavity throughout life, providing a record of growth both before and after eruption of the tooth and allowing precise estimation of age at death[24]. Approximately 75 daily growth increments separate the neonatal line and the pulp cavity in each tooth of this juvenile skeleton, indicating an age at death of approximately 2.5 months for this individual. Despite its young age, the presence of dental mesowear and microwear[39] (Extended Data Fig. 3) in this individual shows that solid foods (not only milk) were being ingested, providing an upper constraint of 75 days on the onset of weaning.

Aligning daily growth records in the teeth based on the neonatal lines enabled the reconstruction of a dental chronology (Fig. 1l). Crown formation times in the teeth were rapid, ranging from 68 to 183 days (approximately 2–6 months; Extended Data Table 1). All of the deciduous teeth were complete and began erupting before birth, and the first and second adult molars had begun mineralizing. The adult molar crowns were completed within 4 months after birth and would have begun erupting in the first year. On the basis of the eruption sequences in other pantodonts[40–42], in which the third molar erupts last, it is therefore likely that all of the adult teeth of *P. bathmodon* erupted within the first year (see Supplementary Information).

In the permanent teeth of mammals, age at death can be estimated from annual bands in the cementum that anchors the tooth to the jaw[24,34]. Cementum annulations were clearly present in the acellular cementum of most teeth in our sample (Fig. 1d). Most individuals had between two and four annual pairs (Extended Data Table 1), but three individuals with highly worn dentitions compared with other Palaeocene pantodonts had five, seven and possibly as many as 11 pairs, respectively (Extended Data Fig. 5; see Supplementary Information).

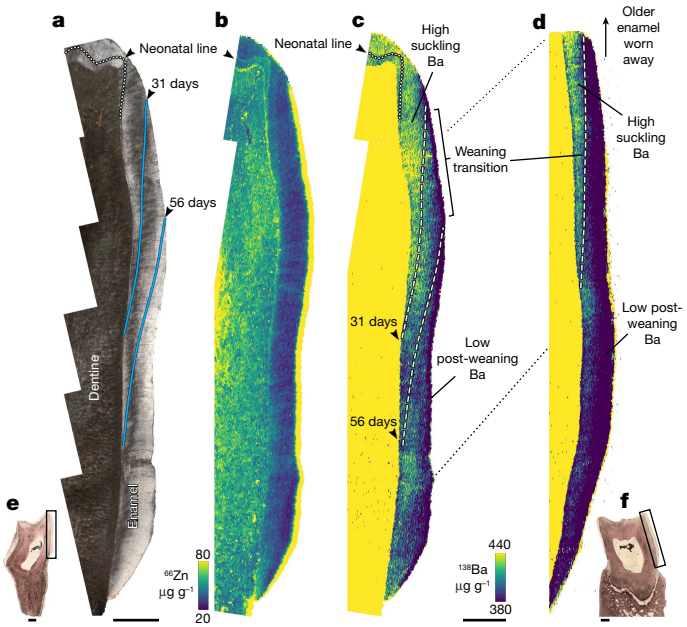

Fig. 2 | Trace element distributions in the enamel of the first and second lower molars (NMMNH P-19541). a, Thin section under cross-polarized light shows clear daily laminations and the neonatal line (dotted line) in the enamel of the paraconid of the second lower molar. **b**, Trace element map of Zn shows enrichment at the neonatal line. **c**, Ba is enriched in early postnatal enamel (also see Supplementary Fig. 8), but decreases gradually between 31 and 56 days after birth (dashed lines). **d**, The transition between high and low levels of Ba is clearer in the paraconid of the first lower molar of the same individual, where older enamel including the neonatal line has been worn away. **e**,**f**, Overview images showing the position of images within the first (**f**) and second (**e**) lower molars. Scale bars, 500 µm (**a**–**d**) and 1 mm (**e**,**f**). See also Supplementary Figs. 1–3.

Skeletal growth

The bone microstructure of the juvenile skeleton (NMMNH P-27844) exhibits densely vascularized fibrolamellar bone, indicating relatively rapid growth (Fig. 1i–k). No annual growth marks are present, consistent with its dental age of approximately 2.5 months, but a band of more organized, slowly growing parallel-fibred bone occurs towards the outer surface of the radius and tibia (Fig. 1i and Extended Data Fig. 6), at an estimated mass of 9 kg (see Supplementary Information). External to this band, the bone shows reduced vascularity and relatively slower growth, on the basis of a higher proportion of parallel-fibred matrix (Fig. 1j,k), although laminations in this tissue are not as well developed as in the lamellar bone of the adult individual. This transition probably corresponds to changes in growth rate associated with weaning, as in living ungulates, a similar transition occurs in some individuals over this interval[43] (see Supplementary Information). The position of this transition partway through the cortex provides evidence for weaning in this individual before death at 2.5 months of age, supporting the 1–2 month suckling period suggested by dental trace elements and tooth wear.

In a skeletally mature adult (NMMNH P-22012), seven annual growth marks were discernible in the exterior cortical bone, matching the number of cementum annulations in its teeth and demonstrating that it was 7 years of age when it died. The exterior cortex is formed of highly organized lamellar bone, indicating slow growth (Fig. 1h). The earliest annual growth mark is within the slowly growing exterior cortex (Extended Data Fig. 7), indicating that growth rate decreased substantially before the end of the first year of life. This probably corresponds to the achievement of sexual maturity[31], suggesting that *P. bathmodon* probably reached sexual maturity and approached maximum body size in its first year.

Life history in *P. bathmodon*

Correcting for the onset of tooth mineralization partway through fetal development (see Supplementary Information), the prenatal growth record in the deciduous teeth indicates a gestation period of roughly 207 days or 29.5 weeks. This is an order of magnitude longer than in marsupials or monotremes, but falls close to extant placentals of similar body size (Fig. 3b). Within placentals, gestation length is dichotomous between species that give birth to single or multiple young in each litter[44] (Fig. 3c). The long gestation period in *P. bathmodon* suggests that it was likely (posterior probability = 0.96) to have given birth to singleton offspring (see Supplementary Information).

Multiple independent lines of evidence from two individuals indicate the onset of weaning between 1 and 2 months after birth in *P. bathmodon*. Postnatal enrichment in enamel Ba for 1–2 months after birth in an adult individual (Fig. 2c,d) is consistent with the development of abrasive microwear and mesowear on the dentition of the juvenile 2.5 months of age (Extended Data Fig. 3) and with the transition recorded in its limb bones (Extended Data Fig. 6), identical to weaning transitions recently described on the basis of fluorescent labelling[43]. Together, these lines of evidence constrain weaning in *P. bathmodon* to between 31 and 75 days after birth, with the weight of evidence supporting cessation of suckling by 2 months after birth. The age (31–75 days) and mass (9 kg) at

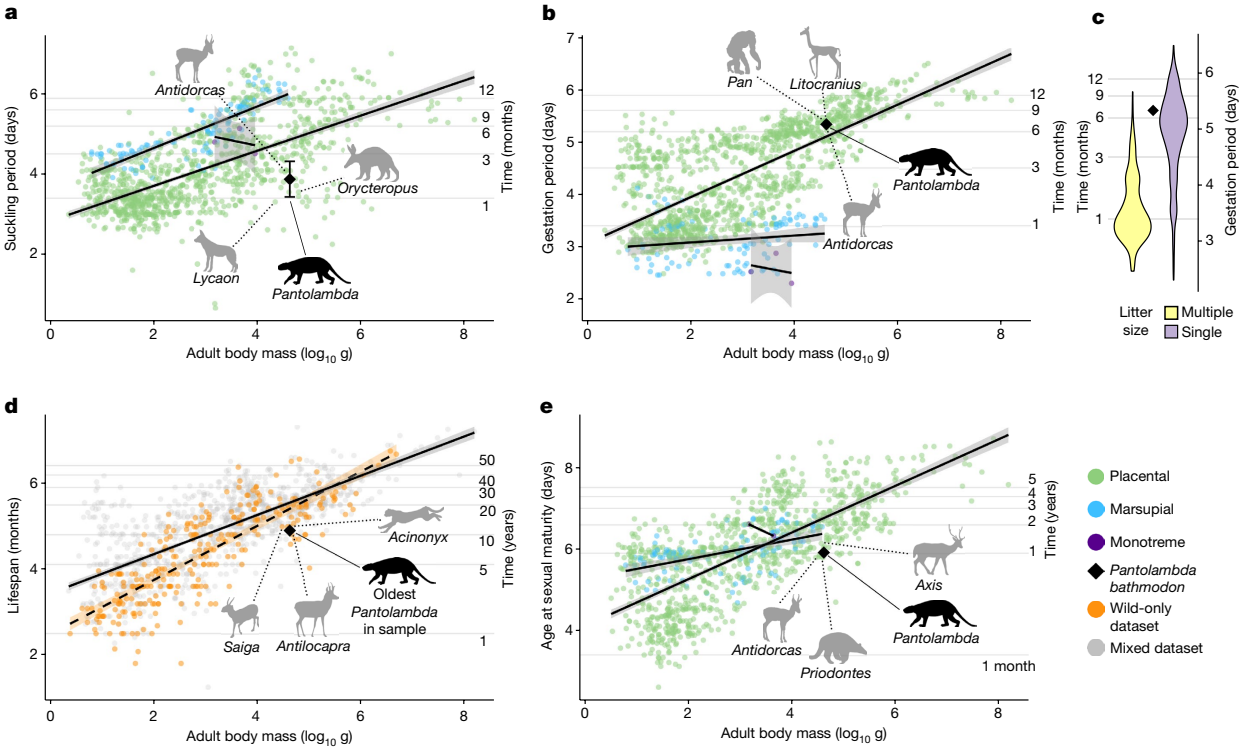

Fig. 3 | Comparison of the reconstructed life history of *P. bathmodon* to extant mammals using the PanTHERIA dataset[50]. **a**, Suckling period showing the range (31–75 days; error bars) estimated for *P. bathmodon* based on dental trace elements, bone histology and dental wear. **b**, Gestation period. **c**, Violin plot of the gestation period sorted by litter size. **d**, Maximum lifespan showing data from PanTHERIA (grey solid line) and from the wild-only lifespan dataset of Newham et al.[34] (orange dashed regression line). **e**, Age at sexual maturity for living mammals (placentals, marsupials and monotremes) plotted against adult body mass (log_{10} mass in grams). Trend lines show generalized linear model regressions for placentals, marsupials and monotremes, with 95% confidence intervals for the regression indicated by shaded envelopes. Horizontal lines show untransformed values. Silhouettes for each panel show living taxa similar in the reconstructed parameter to the estimate for *P. bathmodon*. The silhouette of *P. bathmodon* was created by S.L.S. The silhouettes of *Acinonyx*, *Antilocapra*, *Lycaon*, *Orycteropus*, *Pan* and *Priodontes* were adapted from Phylopic images (CC0 1.0; https://creativecommons.org/publicdomain/zero/1.0/). The silhouette of *Litocranius* was original artwork by G.F.F. All other silhouettes were generated from public domain images (CC0 1.0; https://creativecommons.org/publicdomain/zero/1.0/).

weaning in *P. bathmodon* were shorter and smaller than expected for a placental of its adult body mass, but its gestation period (207 days) was slightly longer (Fig. 3a,b). This indicates greater prenatal than postnatal investment in the young, characteristic of placental mammals[7], but also suggests a distinct life history for these early Palaeocene placentals, consistent with other unusual aspects of their biology[45].

Most individuals within our sample died between 2 and 5 years of age (Fig. 1l), suggesting high mortality in young animals. The oldest specimen in our sample (estimated to be approximately 11 years of age) lived only half the expected lifespan for a mammal of its body mass (20 years; Fig. 3d). This high mortality, in conjunction with its short suckling period and rapid onset of sexual maturity (Fig. 3a,e), suggests a fast pace of life in *P. bathmodon*, despite its relatively large size (42 kg).

Combined with its rapid dental and skeletal development, these life history parameters indicate a highly precocial lifestyle in *P. bathmodon*, comparable with the most precocial extant mammals (for example, deer, giraffes and sheep), which give birth to young with hair and open eyes[13,14]. After a long gestation—the hallmark of the typical placental reproductive mode—a mother *P. bathmodon* probably gave birth to a single, haired offspring with open eyes and well-developed dentition, which was nursed for 1–2 months. At approximately 62 Ma, this constitutes the earliest example of a placentalian-grade physiology in the fossil record.

Growth in early placentals

The growth pattern and rate of *P. bathmodon* differs from those of both Mesozoic mammaliaforms[19,34] and other Cenozoic mammals[46,47]. The mammaliaform *Morganucodon* grew at a much slower rate and for a longer period, evidence of a protracted life history more like that of reptiles than of mammals[19,34]. Late Cretaceous multituberculates and some eutherians had faster growth rates than *Morganucodon*, but these were still not as rapid as extant mammals[19]. By contrast, *P. bathmodon* exhibits fast growth rates and a rapid developmental schedule, more similar to living precocial placentals. Nonetheless, *P. bathmodon* lived and died faster than expected for a mammal of its body size, outpacing extant mammals and even other extinct mammals from later in the Cenozoic[46,47]. The closest living analogues for *Pantolambda*, independent of mass (Extended Data Fig. 8a), are small antelope, such as the neotragines *Madoqua* (Dik-dik) and *Raphicerus* (Steenbok). However, when adult body mass is considered, *Pantolambda* is unique among terrestrial mammals (Extended Data Fig. 8b). This life history strategy would have enabled *P. bathmodon* to proliferate at a rapid rate for an animal of its size, which may have been advantageous in the recovering ecosystems of the Palaeocene. Perhaps, as was the case with locomotion[45] and brain size[48], placental life history strategies became limited to their modern range later, as ecosystems saturated.

In contrast to its distinctly rapid pace of life, the gestation period of *P. bathmodon* is remarkably similar to living placentals of its body mass (Fig. 3b and Extended Data Fig. 8), suggesting a more constrained relationship between size and gestation. Indeed, neonate weight and adult body mass are more tightly correlated than other life history parameters in extant placentals (Extended Data Fig. 9), suggesting that neonate weight drives and/or is constrained by adult body mass. As longer gestation enables the larger neonate sizes required for larger

adults (Extended Data Fig. 9c), extended gestation periods such as that in *P. bathmodon* may have contributed to the rapid increase in body mass in early Palaeocene placentals. The option of extended gestation may have reduced developmental constraints on body size and allowed placentals to expand into vacant niches after the extinction of the non-avian dinosaurs, reaching larger sizes than any Mesozoic mammal[22] and culminating in the largest animals ever[49].

The excellent preservation of daily incremental structures and dietary trace element signatures in a fossil approximately 62 million years of age unlock a new perspective for studying the life history of extinct mammals. Our results suggest that biogenic trace element signals can be retained much longer than previously realized, providing new tools for inferring birth and early-life diet in ancient fossil mammals. Rather than being a limitation for studying reproduction, the abundantly preserved isolated teeth of Mesozoic mammals may enable combined palaeohistological and geochemical approaches to directly address the evolution of reproduction in mammals, including its role in their survival at the end-Cretaceous extinction and their radiation thereafter. Indeed, the highly precocial life history of *P. bathmodon* shows that the physiology of at least some close placental relatives had diverged from other mammals by at least the Palaeocene, early in their evolutionary history[21], and suggests that the capacity to increase body size had a role in their ascent from humble Mesozoic beginnings to the dominant role they have in global ecosystems today.

Online content

Any methods, additional references, Nature Research reporting summaries, source data, extended data, supplementary information, acknowledgements, peer review information; details of author contributions and competing interests; and statements of data and code availability are available at https://doi.org/10.1038/s41586-022-05150-w.

1. Simpson, G. G. The beginning of the age of mammals. *Biol. Rev.* **12**, 1–46 (1937).
2. Grossnickle, D. M., Smith, S. M. & Wilson, G. P. Untangling the multiple ecological radiations of early mammals. *Trends Ecol. Evol.* **34**, 936–949 (2019).
3. Halliday, T. J. D. & Goswami, A. Eutherian morphological disparity across the end-Cretaceous mass extinction. *Biol. J. Linn. Soc.* **118**, 152–168 (2016).
4. Alroy, J. The fossil record of North American mammals: evidence for a Paleocene evolutionary radiation. *Syst. Biol.* **48**, 107–118 (1999).
5. Slater, G. J. Phylogenetic evidence for a shift in the mode of mammalian body size evolution at the Cretaceous–Palaeogene boundary. *Methods Ecol. Evol.* **4**, 734–744 (2013).
6. Williamson, T. E., Brusatte, S. L., Carr, T. D., Weil, A. & Standhardt, B. R. The phylogeny and evolution of Cretaceous–Palaeogene metatherians: cladistic analysis and description of new early Palaeocene specimens from the Nacimiento Formation, New Mexico. *J. Syst. Palaeontol.* **10**, 625–651 (2012).
7. Langer, P. The phases of maternal investment in eutherian mammals. *Zoology* **111**, 148–162 (2008).
8. Lillegraven, J. A., Thompson, S. D., McNab, B. K. & Patton, J. L. The origin of eutherian mammals. *Biol. J. Linn. Soc.* **32**, 281–336 (1987).
9. Austin, C. et al. Barium distributions in teeth reveal early-life dietary transitions in primates. *Nature* **498**, 216–219 (2013).
10. Joannes-Boyau, R. et al. Elemental signatures of *Australopithecus africanus* teeth reveal seasonal dietary stress. *Nature* **572**, 112–115 (2019).
11. Burgin, C. J., Colella, J. P., Kahn, P. L. & Upham, N. S. How many species of mammals are there? *J. Mammal.* **99**, 1–14 (2018).
12. Lillegraven, J. A. Biological considerations of the marsupial–placental dichotomy. *Evolution* **29**, 707–722 (1975).
13. Werneburg, I., Laurin, M., Koyabu, D. & Sánchez-Villagra, M. R. Evolution of organogenesis and the origin of altriciality in mammals: mammalian embryology. *Evol. Dev.* **18**, 229–244 (2016).
14. Ferner, K., Schultz, J. A. & Zeller, U. Comparative anatomy of neonates of the three major mammalian groups (monotremes, marsupials, placentals) and implications for the ancestral mammalian neonate morphotype. *J. Anat.* **231**, 798–822 (2017).
15. Cooper, W. J. & Steppan, S. J. Developmental constraint on the evolution of marsupial forelimb morphology. *Aust. J. Zool.* **58**, 1–15 (2010).
16. Fabre, A.-C. et al. Functional constraints during development limit jaw shape evolution in marsupials. *Proc. R. Soc. B* **288**, 20210319 (2021).
17. Simmons, N. B., Seymour, K. L., Habersetzer, J. & Gunnell, G. F. Primitive early Eocene bat from Wyoming and the evolution of flight and echolocation. *Nature* **451**, 818–821 (2008).
18. Thewissen, J. G. M., Williams, E. M., Roe, L. J. & Hussain, S. T. Skeletons of terrestrial cetaceans and the relationship of whales to artiodactyls. *Nature* **413**, 277–281 (2001).
19. Chinsamy, A. & Hurum, J. H. Bone microstructure and growth patterns of early mammals. *Acta Palaeontol. Pol.* **51**, 325–338 (2006).
20. Novacek, M. J. et al. Epipubic bones in eutherian mammals from the Late Cretaceous of Mongolia. *Nature* **389**, 483–486 (1997).
21. O'Leary, M. A. et al. The placental mammal ancestor and the post-K-Pg radiation of placentals. *Science* **339**, 662–667 (2013).
22. Smith, F. A. et al. The evolution of maximum body size of terrestrial mammals. *Science* **330**, 1216–1219 (2010).
23. Shelley, S. L., Williamson, T. E. & Brusatte, S. L. The osteology of *Periptychus carinidens*: a robust, ungulate-like placental mammal (Mammalia: Periptychidae) from the Paleocene of North America. *PLoS ONE* **13**, e0200132 (2018).
24. Klevezal, G. A. *Recording Structures of Mammals: Determination of Age and Reconstruction of Life History* (Balkema, 1996).
25. Padian, K. & Lamm, E.-T. *Bone Histology of Fossil Tetrapods: Advancing Methods, Analysis, and Interpretation* (Univ. California Press, 2013).
26. Smith, T. M., Cook, L., Dirks, W., Green, D. R. & Austin, C. Teeth reveal juvenile diet, health and neurotoxicant exposure retrospectively: what biological rhythms and chemical records tell us. *BioEssays* **43**, e2000298 (2021).
27. Nacarino-Meneses, C. & Köhler, M. Limb bone histology records birth in mammals. *PLoS ONE* **13**, e0198511 (2018).
28. Köhler, M., Marín-Moratalla, N., Jordana, X. & Aanes, R. Seasonal bone growth and physiology in endotherms shed light on dinosaur physiology. *Nature* **487**, 358–361 (2012).
29. de Margerie, E. Assessing a relationship between bone microstructure and growth rate: a fluorescent labelling study in the King Penguin chick (*Aptenodytes patagonicus*). *J. Exp. Biol.* **207**, 869–879 (2004).
30. Castanet, J., Cubo, J. & Montes, L. Relationship between bone growth rate and bone tissue organization in amniotes: first test of Amprino's rule in a phylogenetic context. *Anim. Biol.* **60**, 25–41 (2010).
31. Calderón, T., DeMiguel, D., Arnold, W., Stalder, G. & Köhler, M. Calibration of life history traits with epiphyseal closure, dental eruption and bone histology in captive and wild red deer. *J. Anat.* **235**, 205–216 (2019).
32. Dirks, W., Humphrey, L. T., Dean, M. C. & Jeffries, T. E. The relationship of accentuated lines in enamel to weaning stress in juvenile baboons (*Papio hamadryas anubis*). *Folia Primatol. (Basel)* **81**, 207–223 (2010).
33. Schwartz, G. T., Reid, D. J., Dean, M. C. & Zihlman, A. L. A faithful record of stressful life events preserved in the dental development record of a juvenile gorilla. *Int. J. Primatol.* **27**, 1221–1222 (2006).
34. Newham, E. et al. Reptile-like physiology in Early Jurassic stem-mammals. *Nat. Commun.* **11**, 5121 (2020).
35. Dean, M. C., Spiers, K. M., Garrevoet, J. & Le Cabec, A. Synchrotron X-ray fluorescence mapping of Ca, Sr and Zn at the neonatal line in human deciduous teeth reflects changing perinatal physiology. *Arch. Oral Biol.* **104**, 90–102 (2019).
36. Smith, T. M. et al. Permanent signatures of birth and nursing initiation are chemically recorded in teeth. *J. Archaeol. Sci.* **140**, 105564 (2022).
37. Tafforeau, P., Bentaleb, I., Jaeger, J.-J. & Martin, C. Nature of laminations and mineralization in rhinoceros enamel using histology and X-ray synchrotron microtomography: potential implications for palaeoenvironmental isotopic studies. *Palaeogeogr. Palaeoclimatol. Palaeoecol.* **246**, 206–227 (2007).
38. Schour, I. The neonatal line in the enamel and dentin of the human deciduous teeth and first permanent molar. *J. Am. Dent. Assoc.* **23**, 1946–1955 (1936).
39. Scott, R. M. & Halcrow, S. E. Investigating weaning using dental microwear analysis: a review. *J. Archaeol. Sci. Rep.* **11**, 1–11 (2017).
40. Mao, F., Wang, Y.-Q., Meng, J. & Jin, X. Tooth crown formation time in three Asian coryphodontids, and its implication for identifying living analogues. *Vertebr. Palasiat.* **42**, 153–170 (2014).
41. Lucas, S. G. & Schoch, R. M. Ontogenetic studies of early Cenozoic *Coryphodon* (Mammalia, Pantodonta). *J. Paleontol.* **64**, 831–841 (1990).
42. Muizon, C. de & Marshall, L. G. *Alcidedorbignya inopinata* (Mammalia: Pantodonta) from the Early Paleocene of Bolivia: phylogenetic and paleobiogeographic implications. *J. Paleontol.* **66**, 499–520 (1992).
43. Calderón, T., Arnold, W., Stalder, G., Painer, J. & Köhler, M. Labelling experiments in red deer provide a general model for early bone growth dynamics in ruminants. *Sci Rep.* **11**, 14074 (2021).
44. Müller, D. W. H. et al. Dichotomy of eutherian reproduction and metabolism. *Oikos* **121**, 102–115 (2012).
45. Shelley, S. L., Brusatte, S. L. & Williamson, T. E. Quantitative assessment of tarsal morphology illuminates locomotor behaviour in Palaeocene mammals following the end-Cretaceous mass extinction. *Proc. R. Soc. B* **288**, 20210393 (2021).
46. Kolb, C. et al. Mammalian bone palaeohistology: a survey and new data with emphasis on island forms. *PeerJ* **3**, e1358 (2015).
47. Dirks, W., Anemone, R. L., Holroyd, P. A., Reid, D. J. & Walton, P. in *Comparative Dental Morphology* Vol. 13 (eds. Meyer, G., Koppe, T. & Alt, K. W.) 3–8 (Karger, 2009).
48. Bertrand, O. C. et al. Brawn before brains in placental mammals after the end-Cretaceous extinction. *Science* **376**, 80–85 (2022).
49. Smith, F. A. & Lyons, S. K. How big should a mammal be? A macroecological look at mammalian body size over space and time. *Phil. Trans. R. Soc. B* **366**, 2364–2378 (2011).
50. Jones, K. E. et al. PanTHERIA: a species-level database of life history, ecology, and geography of extant and recently extinct mammals. *Ecology* **90**, 2648–2648 (2009).

Methods

We prepared thin sections (see Supplementary Information) of the teeth and bones of 12 specimens of *P. bathmodon*, including two partial skeletons and totalling 45 elements (23 bones and 22 teeth), collected from the Torrejonian NALMA of the Nacimiento Formation in the San Juan Basin of New Mexico, USA[51]. The specimens were selected to represent as much of the skeleton and as many tooth positions as possible and to capture varying degrees of dental wear, presumably attributable to individuals of different ages. No statistical method was used to determine sample size and specimen analysis was not randomized or blinded. The minimum number of individuals based on skeletal overlap a priori was three, but age variation indicated a minimum of seven individuals in our palaeohistological sample.

Incremental marks in the cementum, dentine and enamel were counted from thin sections to assess the timing and pace of tooth development. Cementum annulations, lines of von Ebner in the dentine and cross-striations in the enamel were each clearly visible under cross-polarized light. Pairs of one light and one dark band in the acellular extrinsic fibre cementum near the cervix of the tooth were counted as growth layer groups representing annual growth cycles[24,52,53]. Lines of von Ebner in the dentine, clearly distinct from more broadly spaced Andresen lines[24,54], were counted from high-magnification photomontages as daily increments of growth. Likewise, cross-striations in the enamel were interpreted as daily increments of growth[54,55]. In every specimen, enamel cross-striations were aligned into clearly visible growth laminations, which have a daily periodicity[37,56]. The neonatal line in the enamel was identified as a prominent, Zn-enriched[35] accentuated line formed by discontinuities in the enamel prisms. In the dentine of the deciduous teeth, the earliest accentuated stress line was identified as the neonatal line[24], which was supported by consistent changes in Zn concentration across the neonatal boundary[35,57] (Extended Data Fig. 4). The neonatal line was used to demarcate prenatal and postnatal developmental periods, and to align sequences from different tooth positions within and between individuals. Daily growth increments in the enamel were traced from high-resolution photomontages to create temporal maps of daily dental development for each tooth. Enamel secretion, crown extension and crown formation rates were estimated using previously published methods[47].

Dietary trace element concentrations were assessed using laser ablation inductively coupled plasma mass spectroscopy (LA–ICP–MS) at the University of Edinburgh and the University of St Andrews Isotope Geochemistry (STAiG) laboratory. After pilot runs using an ATLEX-I-LR Analyte Excite 193 nm ArF excimer coupled to an Attom ICPMS, Nu Instrument at the University of Edinburgh, to assess the suitability of the material for analysis, a broad array of trace element concentrations (^{11}B, ^{23}Na, ^{25}Mg, ^{27}Al, ^{31}P, ^{43}Ca, ^{46}Ca, ^{55}Mn, ^{59}Co, ^{60}Ni, ^{63}Cu, ^{66}Zn, ^{88}Sr, ^{89}Y, ^{138}Ba, ^{208}Pb and ^{238}U) in the enamel and dentine of six teeth were mapped using LA–ICP–MS on an Agilent 8900-QQQ at the STAiG laboratory. Entire enamel sequences of three teeth (the paraconid of a lower first molar (NMMNH P-19541), the protoconid of a lower second molar (NMMNH P-19541) and the labial enamel of an incisor (NMMNH P-69918)) were scanned at high resolution (20-μm spot size, 10 μm s^{-1} scanning speed and inductively coupled plasma cycle time of 0.2889 s), with an effective pixel size of 60 μm^2 (Supplementary Figs. 1–4). Small regions of interest in the deciduous teeth (NMMNH P-27844) were also scanned at high resolution (38-μm spot size and 38 μm s^{-1} scanning speed; Supplementary Figs. 5–7). LA–ICP–MS data were processed and rasterized in Iolite v4.5.5.4 (ref. [58]). Concentrations were normalized to and drift-corrected by a National Institute of Standards and Technology 612 glass standard after gas blank subtraction, and standardized to approximately 40% Ca. Elemental maps and transects were registered to temporal maps of dental development to evaluate daily changes in diet.

Dental microwear was evaluated using scanning electron microscopy using a Carl Zeiss SIGMA DH VP field emission scanning electron microscope at the University of Edinburgh operated at 15 kV for secondary electron imaging of the fine-scale features of the occlusal surface of the first upper molar of NMMNH P-27844.

Reconstructed life history parameters for *P. bathmodon* were plotted alongside data from the PanTHERIA dataset[50] for comparison. Because the PanTHERIA dataset includes mostly captive individuals, which are likely to have greater maximum lifespans than wild individuals, the estimated maximum lifespan of *P. bathmodon* was also compared with a recent wild-only dataset of mammal maximum lifespan[34]. Relative importance of life history parameters for predicting body size was evaluated using multiple regression, and litter size was predicted using linear discriminant analysis based on gestation period. Principal components analysis was used to identify the closest living analogues of *P. bathmodon*.

Reporting summary

Further information on research design is available in the Nature Research Reporting Summary linked to this article.

Data availability

Fossil specimens in this study are housed at the NMMNH, and the palaeohistological thin sections underlying the analyses are accessioned at the University of Edinburgh but will be returned to the NMMNH for permanent curation upon completion of our research. The living mammal datasets are available from Jones et al.[50] (https://doi.org/10.6084/m9.figshare.c.3301274.v1) and Newham et al.[34] (https://www.nature.com/articles/s41467-020-18898-4#Sec18). Overview images of palaeohistological slides and LA–ICP–MS data are deposited at Figshare (https://doi.org/10.6084/m9.figshare.20272737). Source data are provided with this paper.

Code availability

No custom code or software was used in the study.

51. Williamson, T. E. The beginning of the Age of Mammals in the San Juan Basin, New Mexico: biostratigraphy and evolution of Paleocene mammals of the Nacimiento Formation: bulletin 8. *New Mexico Mus. Nat. Hist. Sci. Bull.* **8**, 1–141 (1996).
52. Newham, E. et al. Synchrotron radiation-based X-ray tomography reveals life history in primate cementum incrementation. *J. R. Soc. Interface* **17**, 20200538 (2020).
53. Berkovitz, B. & Shellis, P. *The Teeth of Mammalian Vertebrates* 305–321 (Elsevier, 2018).
54. Dean, M. C. Tooth microstructure tracks the pace of human life-history evolution. *Proc. R. Soc. B* **273**, 2799–2808 (2006).
55. Smith, T. M. Teeth and human life-history evolution. *Annu. Rev. Anthropol.* **42**, 191–208 (2013).
56. Emken, S., Witzel, C., Kierdorf, U., Frölich, K. & Kierdorf, H. Characterization of short-period and long-period incremental markings in porcine enamel and dentine—results of a fluorochrome labelling study in wild boar and domestic pigs. *J. Anat.* **239**, 1207–1220 (2021).
57. Lochner, F., Appleton, J., Keenan, F. & Cooke, M. Multi-element profiling of human deciduous teeth by laser ablation-inductively coupled plasma-mass spectrometry. *Anal. Chim. Acta* **401**, 299–306 (1999).
58. Paton, C., Hellstrom, J., Paul, B., Woodhead, J. & Hergt, J. Iolite: Freeware for the visualisation and processing of mass spectrometric data. *J. Anal. At. Spectrom.* **26**, 2508–2518 (2011).

Acknowledgements We thank N. Volden for facilitating specimen access, J. Craven for access to microscopy facilities and A. Reynolds for discussion of captive lifespan. Funding was provided by the University of Edinburgh, the Royal Society (grant NIF\R1\191527), National Science Foundation (grants DEB 1654949 and EAR 1654952), European Research Council (ERC) starting grants (nos. 756226 and 805246) under the European Union's Horizon 2020 Research and Innovation Programme, a Philip Leverhulme Prize and a SNSF Mobility Fellowship (grant P2EZP2_199923).

Author contributions G.F.F. designed the study, made the thin sections, conducted the histological, life history and statistical analyses, prepared the figures and wrote the manuscript. P.E.d. contributed to the study design, identification of the material, morphological analyses and drafting the manuscript. J.T.S. and M.D. conducted the LA–ICP–MS analyses at STAiG and contributed to figures and drafting the manuscript. S.L.S. created the skeletal reconstruction

of *P. bathmodon* and contributed to discussion and drafting the manuscript. L.E.P. conducted the LA–ICP–MS analyses at the University of Edinburgh and contributed to drafting the manuscript. N.J.C. conducted the scanning electron microscopy analyses. J.R.W. contributed to drafting the manuscript. T.E.W. oversaw the collection and curation of the material, provided stratigraphic data and contributed to drafting the manuscript. J.W.B.R. supervised the LA–ICP–MS analyses. S.L.B. coordinated the project and contributed to study design and drafting the manuscript.

Competing interests The authors declare no competing interests.

Additional information

Supplementary information The online version contains supplementary material available at https://doi.org/10.1038/s41586-022-05150-w.

Correspondence and requests for materials should be addressed to Gregory F. Funston or Stephen L. Brusatte.

Peer review information *Nature* thanks Renaud Joannes-Boyau, Tanya Smith and the other, anonymous, reviewer(s) for their contribution to the peer review of this work. Peer reviewer reports are available.

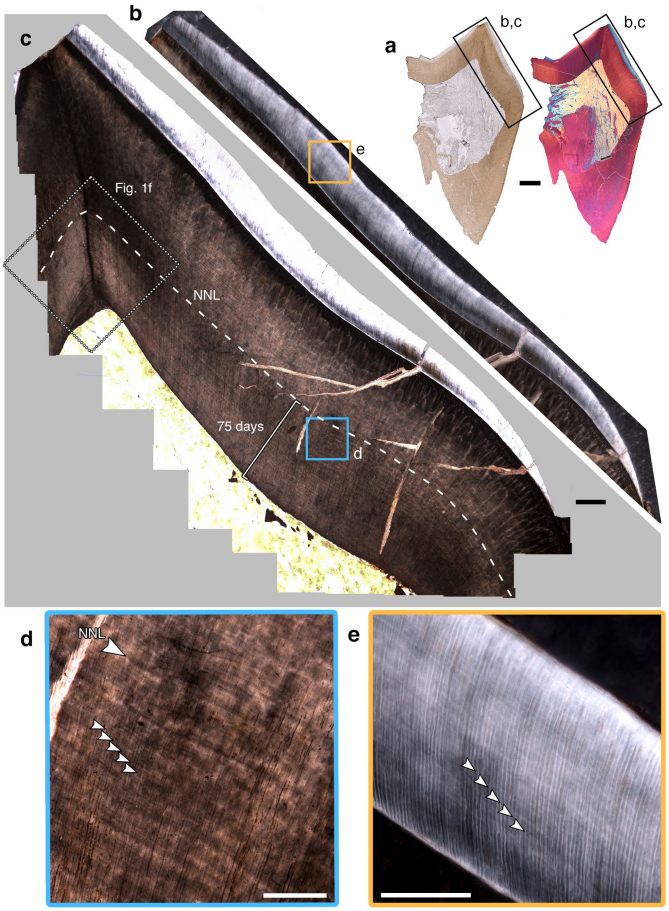

Extended Data Fig. 1 | Incremental features of the teeth of *Pantolambda bathmodon*. (a) Overview of coronal section of deciduous ultimate upper premolar of NMMNH P-27844 under plane-polarized light (left) and cross-polarized light with a lambda filter (right), showing locations of inset images. (b,c) Photomontages of the protocone exposed for the enamel (b) and the dentine (c), showing excellent preservation of incremental features, neonatal line (dashed line), and locations of close-up images. (d) Contrast-enhanced close-up of lines of von Ebner preserved in the dentine (arrows), extending parallel to the dentinoenamel junction and perpendicular to dentine tubules, and neonatal line (large arrow). (e) Contrast-enhanced close-up of enamel cross-striations and daily laminations (arrows) in the enamel, extending sub-parallel to the dentinoenamel junction and perpendicular to the enamel prisms. Images in b–e are under cross-polarized light. **Abbreviations**: **NNL**, neonatal line. Scale bars: 1 mm (a), 200 µm (b, c), 100 µm (d, e).

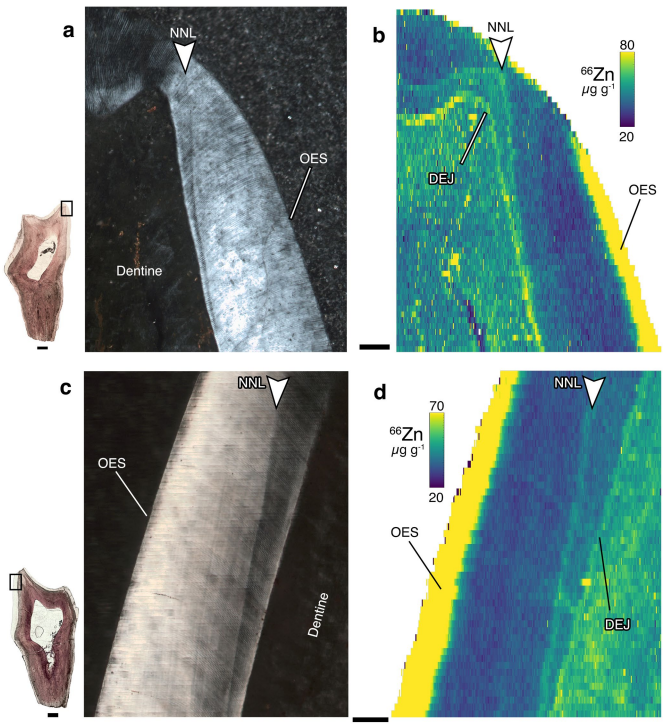

Extended Data Fig. 2 | Zn-enrichment of the neonatal line in the enamel of lower second molar of NMMNH P-19541. (a, c) coronal sections of enamel of paraconid (a) and protoconid (c) under cross-polarized light. Insets show location on coronal sections of entire tooth. (b, d), LA-ICP-MS trace element maps, showing higher concentrations of Zn in discrete areas corresponding to the neonatal line (white arrows). **Abbreviations**: **DEJ**, dentinoenamel junction; **NNL**, neonatal line; **OES**, outer enamel surface. Scale bars: 1 mm (insets), 100 µm (a–d).

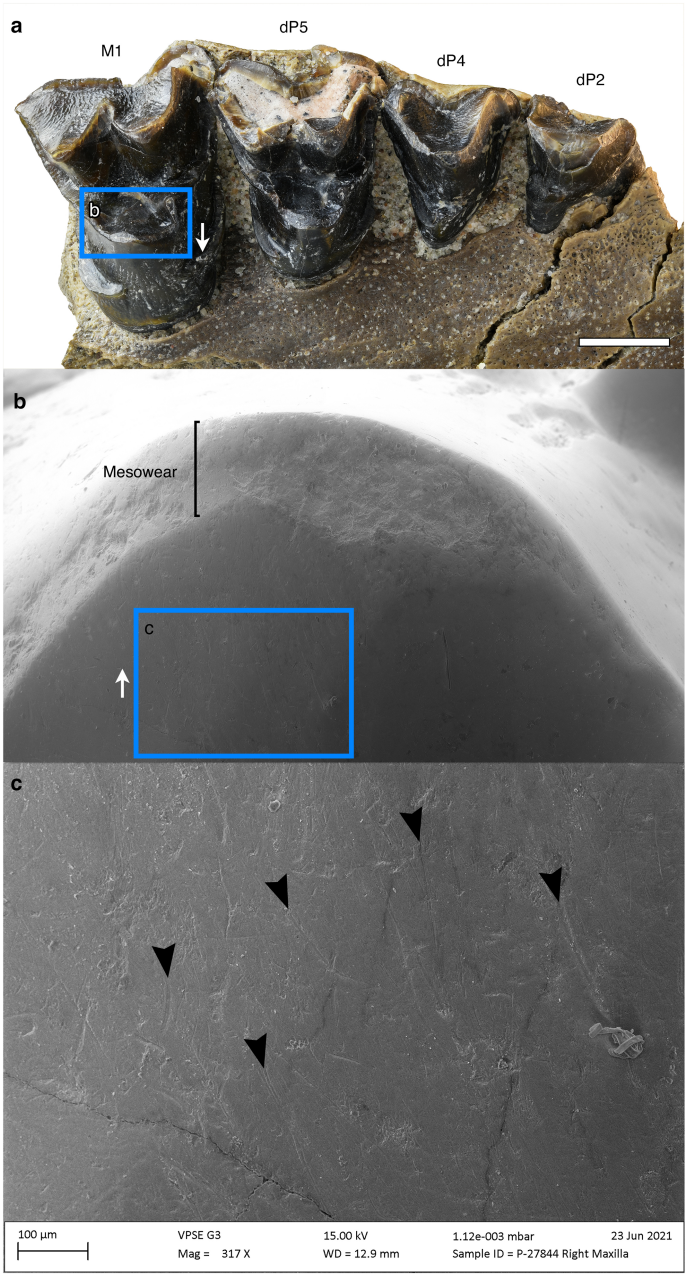

Extended Data Fig. 3 | Microwear on the dentition of NMMNH P-27844. (a) Right maxilla with three deciduous premolars and adult first molar in occlusal view, showing location of scanning electron microscopy (SEM) scan. (b) Overview secondary electron (SE) image of protocone of adult first molar, showing development of mesowear and location of close-up image. (c) Close-up SE image of scratches and gouges attributable to abrasive microwear; black arrows highlight curved scratches resulting from chewing motion. White arrows in (a) and (b) indicate lingual direction. **Abbreviations**: **d**, deciduous; **M**, upper molar; **P**, upper premolar.

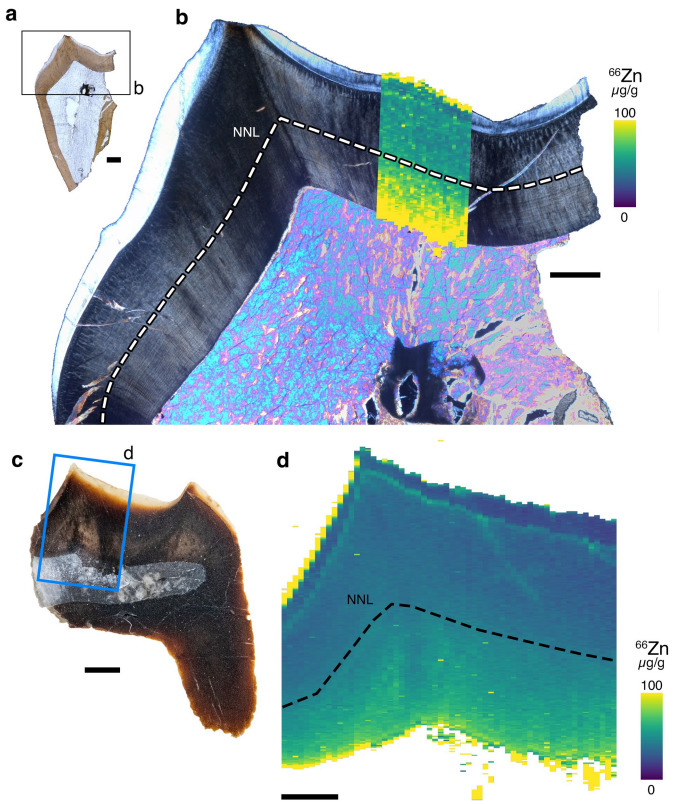

Extended Data Fig. 4 | Changes in zinc associated with birth in the deciduous upper premolars of NMMNH P-27844. Postnatal dentine is enriched in Zn in the deciduous upper ultimate premolar (a, b) and the deciduous upper second premolar (c, d). (a) Overview of thin section showing location of close-up image. (b) Mosaic image showing protocone in cross-polarized light, with trace element map overlain, showing change at histologically-inferred neonatal line (dashed line; NNL). (c) Overview image of embedded block showing location of trace element map. (d) Trace element map showing increased postnatal Zn. Scale bars: 1 mm (a, c), 500 µm (b, d). **Abbreviations**: **NNL**, neonatal line.

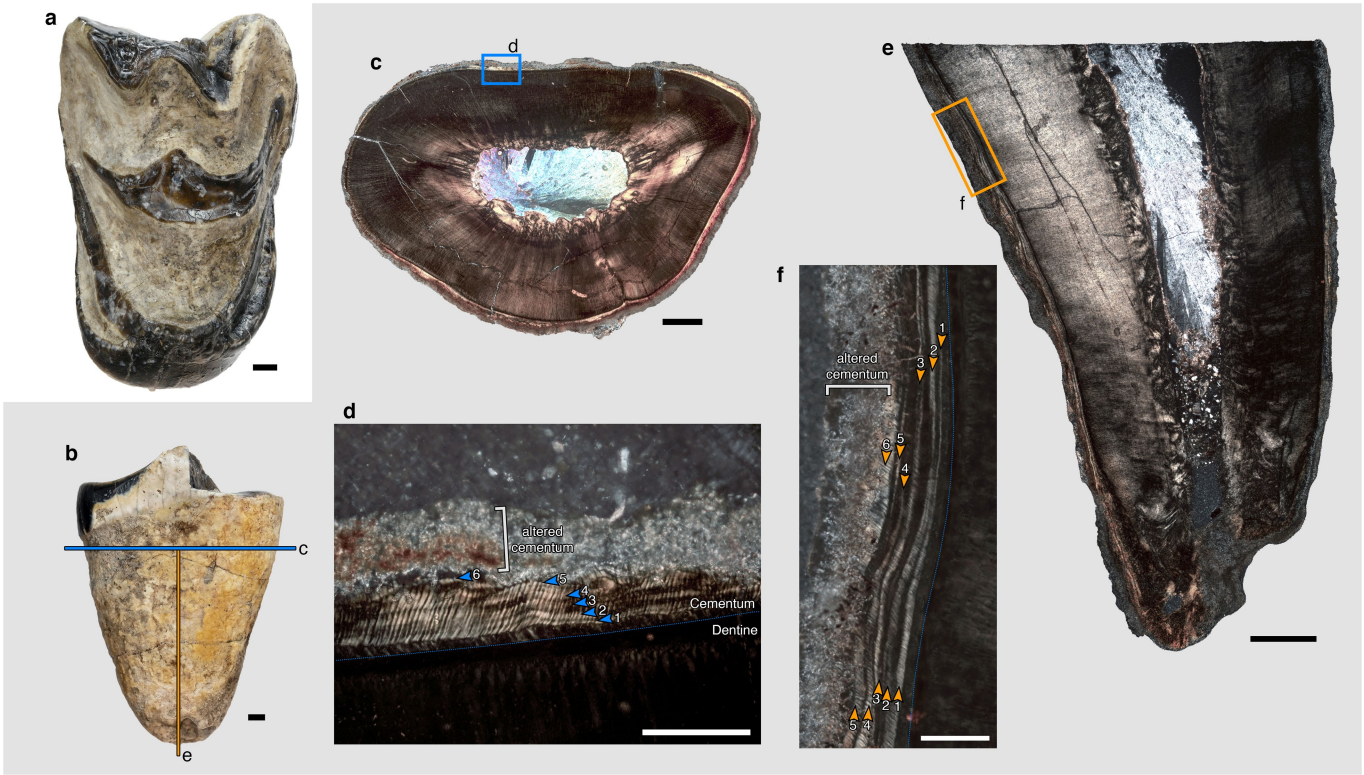

Extended Data Fig. 5 | Dental wear, cementum annulations, and maximum lifespan in the oldest sampled individuals. (a) Right first upper molar of NMMNH P-19625, showing extensive wear and erosion of enamel in most areas of the crown. (b) Anterior root of lower molar (tooth position unknown) from another individual of NMMNH P-19625, showing the location of the thin sections. (c) Overview transverse section of cervical root area, showing clear demarcation of cementum and dentine, and location of close-up. (d) Close-up of acellular extrinsic-fiber cementum in transverse section, showing six pairs of dark and bright bands comprising annual growth layer groups and alteration of external cementum; bright bands indicated with blue arrows. (e) longitudinal section of the same tooth, showing thick external layer of cementum, continuity of growth layer groups, and location of close-up. (f) close-up image of acellular extrinsic-fiber cementum in longitudinal section, showings six annual growth layer groups and alteration of external cementum; bright bands indicated with orange arrows. Images c–f under cross-polarized light. Scale bars: 1 mm (a–c, e), 200 µm (d, f).

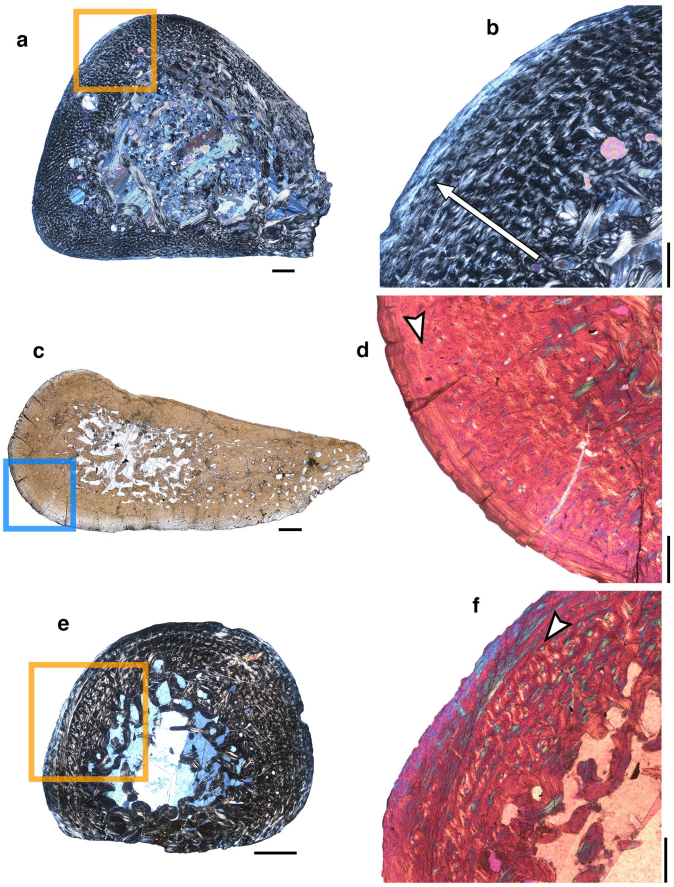

Extended Data Fig. 6 | Weaning transition recorded in the postcranial bones of NMMNH P-27844. (a) Transverse section of right humerus diaphysis under cross-polarized light, showing arrangement of tissues and large medullary cavity and location of close-up image. (b) Close-up of cortex of right humerus under cross-polarized light, showing increase in proportion of parallel-fibered bone (brighter tissues) later in growth (arrow), indicative of a decrease in growth rate. (c) Transverse section of right tibia diaphysis under plane polarized light, showing location of close-up image. (d) Close-up of cortex of right tibia under cross-polarized light with a lambda filter, showing transition (arrow) from highly-vascularized fibrolamellar bone with a high proportion of woven-fibered matrix (upper right) to more slowly-growing parallel-fibered bone with reduced vascularity (lower left). (e) Transverse section of right radius diaphysis under cross-polarized light, showing location of close-up image. (f) Close-up image of cortex of right radius under cross-polarized light with a lambda filter, showing annulus of parallel-fibered bone (arrow) separating region of highly-vascularized fibrolamellar bone (lower right) from region of less-vascularized fibrolamellar bone with a higher proportion of parallel-fibered bone (upper left). Scale bars: 1 mm (a, c, e), 500 µm (b, d, f).

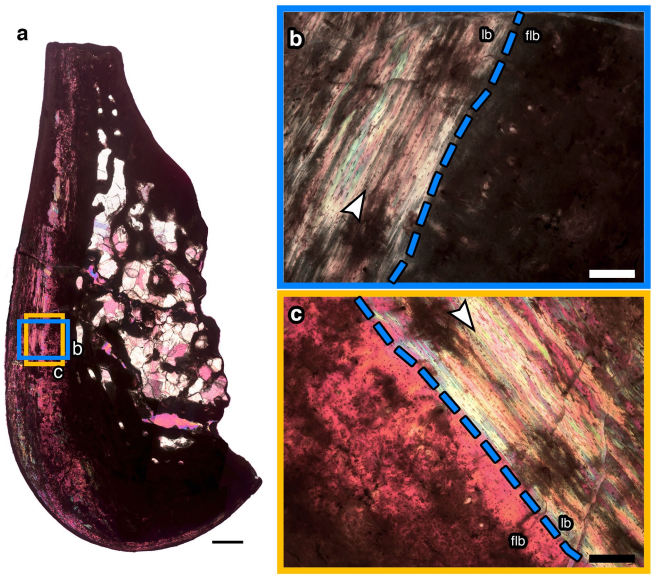

Extended Data Fig. 7 | Transition to slower growth likely reflecting sexual maturity. (a) Coronal section of posterior dentary of NMMNH P-22012 under cross-polarized light with a lambda filter, showing locations of close-up images. Dark regions have been diagenetically altered by the deposition of opaque minerals. (b, c) Close-up of transition (dashed line) between faster-growing fibrolamellar bone (flb) and slower-growing lamellar bone (lb), indicative of sexual maturity, under cross-polarized light (b) and cross-polarized light with a lambda filter (c). Arrows indicate first line of arrested growth, deposited after the transition to slower growth. Scale bars: 1 mm (a), 200 µm (b, c).

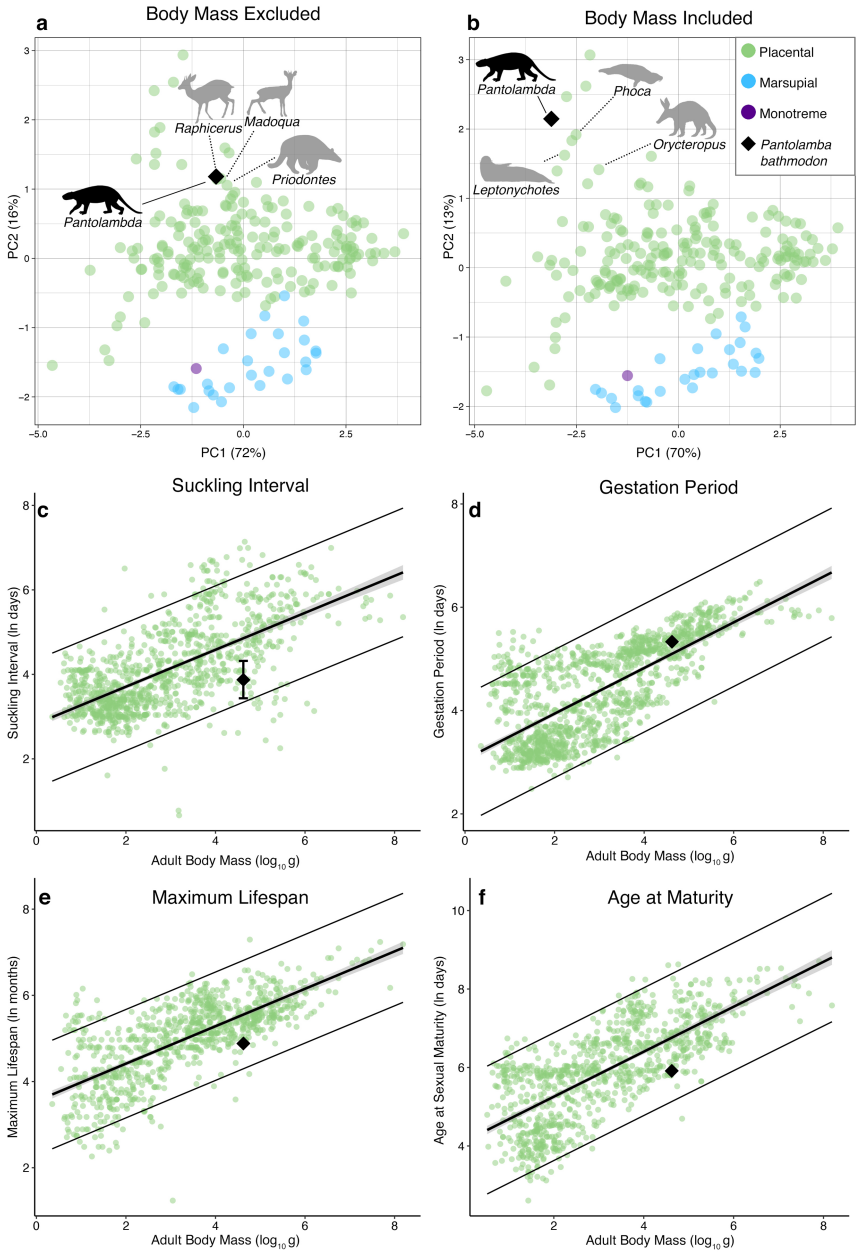

Extended Data Fig. 8 | Life history of *P. bathmodon* compared to living mammals. (a, b) principal components analyses using the PanTHERIA dataset (placentals, green; marsupials, blue; monotremes, purple) incorporating suckling interval, gestation period, maximum lifespan, and age at sexual maturity, with adult body mass excluded (a) or included (b) as a variable; close living analogues to *P. bathmodon* indicated by silhouettes. (c–f) regressions of life history variables in placental mammals with 95% confidence intervals (thin black lines) centred on the generalized linear model regression trendline for suckling interval (c), gestation period (d), maximum lifespan (e), and age at sexual maturity (f), showing that *P. bathmodon* is within the 95% confidence interval of placentals in all parameters. Silhouette of *Pantolambda bathmodon* created by SLS. Silhouettes of *Orycteropus* and *Priodontes* adapted from Phylopic images (CC0 1.0 https://creativecommons.org/publicdomain/zero/1.0/), silhouette of *Leptonychotes* is original artwork by GFF, silhouette of *Phoca* was generated from a photograph taken by GFF, and all others were generated from public domain images (CC0 1.0 https://creativecommons.org/publicdomain/zero/1.0/).

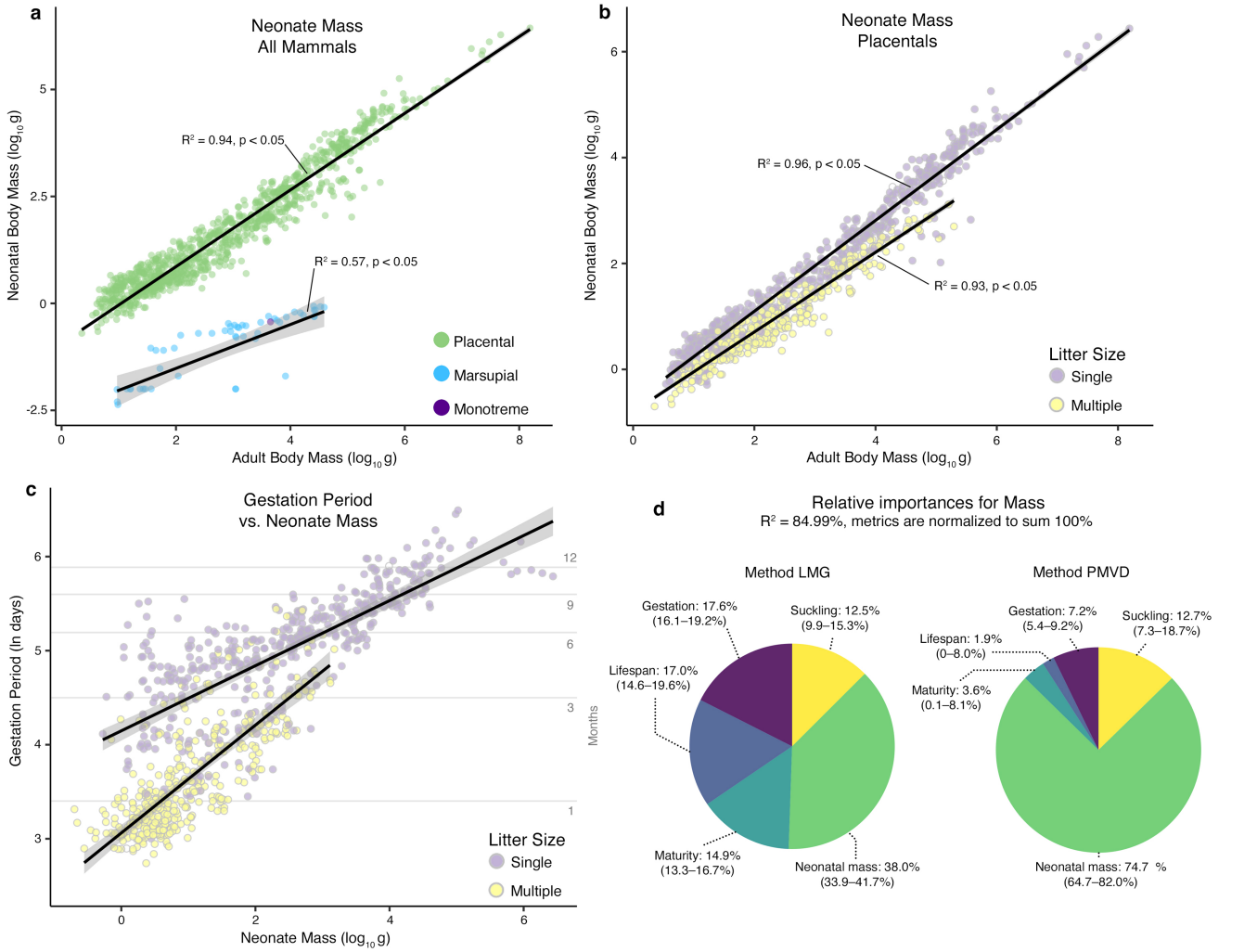

Extended Data Fig. 9 | Relationship between neonate mass and adult body mass in extant mammals. (a) Generalized linear model regression of neonate body mass against adult body mass for all species in the PanTheria dataset, showing clear separation of placental mammals (green, p-value < 2.2×10^{-16}) from non-placental mammals (p-value: 4.07×10^{-6}); 95% confidence interval for regression slope shown as shaded envelope. (b) Neonate body mass plotted against adult body mass for placental species, showing tight correlations of neonate mass and adult mass (p values both < 2.2×10^{-16}); 95% confidence interval for generalized linear model regression slope shown as shaded envelope. (c) Gestation period plotted against neonate body mass; 95% confidence interval for generalized linear regression slope shown as shaded envelope. (d) Relative importance of multiple regression of adult body mass against neonate weight, gestation period, maximum lifespan, time to sexual maturity, and suckling period, showing relative contribution of factors to adult body mass; confidence intervals derived from 1000 replicates of bootstrapping.

Extended Data Table 1 | Quantitative dental histological data for *Pantolambda bathmodon*

Specimen (NMMNH)	Element	Retzius Periodicity	Enamel Secretion Rate (μm/d)	Lamination Angle	Crown Extension Rate (μm/d)	Prenatal Formation Time (d)	Crown Formation Time (d)	Cementum Annulations[§]	Trace Element Analysis
P-19541	Lm1	2	9.3	4.4°	93.5	-	154	3	Protoconid
	Lm2	2	9.9[‡]	7.2°	78[‡]	78	195	2.5	Protoconid and Paraconid
P-19612	C	1	9.3	5.0°	89	-	-	3	-
P-19625	M1	1	-	-	-	-	-	5	-
	Root	-	-	-	-	-	-	11*	-
P-22012	P4	-	-	-	-	-	-	7	-
P-27844	LdP2	1	9.2[†]	4.1°	114[†]	116	68	0.5	Paracone
	LdP4	1	-	-	-	-	-	-	Paracone
	LdP5	1	9.75[†]	5.0°	142[†]	138	98	0.5	Protocone
P-41514	LM1	1	-	-	-	-	-	3	-
	LM2	1	-	-	-	-	-	3	-
	LM3	1	-	-	-	-	-	2.5	-
P-69892	Lm3	2	9.1	9.4	71	-	-	2.5	Pilot transect
P-69918	i	1	7.4	6.4°	70	-	121	3	Labial enamel
P-69919	Lp1	1	10.4	6.1°	78	-	115	4	-
P-69923	I	1	7.0	5.65°	49	-	126	4	-
P-69925	C	1	-	-	-	-	-	3	-

Note: *estimate, see Supplementary Information for further details. For teeth with a neonatal line, [†]prenatal, [‡]postnatal. [§]counted as a pair of light and dark bands; - inapplicable or not available

nature portfolio

Corresponding author(s): Gregory F. Funston

Last updated by author(s): Jul 8, 2022

Reporting Summary

Nature Portfolio wishes to improve the reproducibility of the work that we publish. This form provides structure for consistency and transparency in reporting. For further information on Nature Portfolio policies, see our Editorial Policies and the Editorial Policy Checklist.

Statistics

For all statistical analyses, confirm that the following items are present in the figure legend, table legend, main text, or Methods section.

n/a	Confirmed
☐	☒ The exact sample size (*n*) for each experimental group/condition, given as a discrete number and unit of measurement
☒	☐ A statement on whether measurements were taken from distinct samples or whether the same sample was measured repeatedly
☐	☒ The statistical test(s) used AND whether they are one- or two-sided *Only common tests should be described solely by name; describe more complex techniques in the Methods section.*
☒	☐ A description of all covariates tested
☒	☐ A description of any assumptions or corrections, such as tests of normality and adjustment for multiple comparisons
☐	☒ A full description of the statistical parameters including central tendency (e.g. means) or other basic estimates (e.g. regression coefficient) AND variation (e.g. standard deviation) or associated estimates of uncertainty (e.g. confidence intervals)
☐	☒ For null hypothesis testing, the test statistic (e.g. *F*, *t*, *r*) with confidence intervals, effect sizes, degrees of freedom and *P* value noted *Give P values as exact values whenever suitable.*
☒	☐ For Bayesian analysis, information on the choice of priors and Markov chain Monte Carlo settings
☒	☐ For hierarchical and complex designs, identification of the appropriate level for tests and full reporting of outcomes
☒	☐ Estimates of effect sizes (e.g. Cohen's *d*, Pearson's *r*), indicating how they were calculated

Our web collection on statistics for biologists contains articles on many of the points above.

Software and code

Policy information about availability of computer code

Data collection	Photoshop CC 2021 was used to process image data and to assemble microscopy images into photomontages. Microsoft Excel was used for compiling data including histological measurements, LA-ICP-MS pilot data, and the PanTheria dataset. ImageJ 1.52q was used to take histological measurements.
Data analysis	Iolite v4.5.5.4 software was used to process LA-ICP-MS data. RStudio v3.6.1 was used for all statistical analyses. Packages used include ggplot2, ggplotify, ggpubr, ggsci, gridExtra, MASS, MPSEM, relaimpo, and tidyverse. No custom code was used for data analysis.

For manuscripts utilizing custom algorithms or software that are central to the research but not yet described in published literature, software must be made available to editors and reviewers. We strongly encourage code deposition in a community repository (e.g. GitHub). See the Nature Portfolio guidelines for submitting code & software for further information.

Data

Policy information about availability of data

All manuscripts must include a data availability statement. This statement should provide the following information, where applicable:

- Accession codes, unique identifiers, or web links for publicly available datasets
- A description of any restrictions on data availability
- For clinical datasets or third party data, please ensure that the statement adheres to our policy

Fossil specimens (in this study are housed at the New Mexico Museum of Natural History and Science, and the palaeohistological thin sections underlying the analyses are accessioned at the University of Edinburgh but will be returned to the NMMNH for permanent curation upon completion of our research. The living mammal datasets are available from Jones et al. (ref 51; https://doi.org/10.6084/m9.figshare.c.3301274.v1) and Newham et al. (ref 35; https://www.nature.com/

articles/s41467-020-18898-4#Sec18). Overview images of palaeohistological slides and LA-ICP-MS data are reposited in Figshare (doi: 10.6084/m9.figshare.20272737), where they are publicly available.

Field-specific reporting

Please select the one below that is the best fit for your research. If you are not sure, read the appropriate sections before making your selection.

☐ Life sciences ☐ Behavioural & social sciences ☒ Ecological, evolutionary & environmental sciences

For a reference copy of the document with all sections, see nature.com/documents/nr-reporting-summary-flat.pdf

Ecological, evolutionary & environmental sciences study design

All studies must disclose on these points even when the disclosure is negative.

Study description	The study included the production of palaeohistological thin sections from fossil material, analysis of incremental structures within the thin sections, LA-ICP-MS analysis of trace element distributions in the thin sections, and comparison of these results to a previously-published life history dataset of extant mammals. Quantitative data were not separated into experimental groups nor treated in any way.
Research sample	The research sample included fossil specimens of Pantolambda bathmodon accessioned at the New Mexico Museum of Natural History and Science, and on loan to the University of Edinburgh for morphological analyses. We chose to use specimens from this collection because it is the largest collection of Pantolambda bathmodon available, each specimen has associated locality data, and the specimens were available for consumptive histological sampling. Sampled elements were chosen to represent as many tooth positions as possible, and to represent a variety of ontogenetic stages, based on degrees of skeletal fusion, size, and dental wear. All specimens were collected from the Nacimiento Formation in the San Juan Basin of New Mexico. We used two publicly available datasets for comparison (PanTheria and Newham et al.). The PanTheria dataset was chosen because it is the largest life history dataset of mammals currently available, and it contains data for a wider range of clades and each of the life history variables of interest. We chose the Newham et al. dataset because it is the largest available lifespan dataset for which values derived from wild and captive animals are separate.
Sampling strategy	The sample was chosen based on availability and suitability for destructive sampling. For geochemical sampling, specimens which showed clear incremental growth marks and a distinct neonatal line were selected. LA-ICP-MS scans were created for entire enamel sequences of either the protoconid or paraconid of three teeth, supplemented by targeted sampling of small areas of other teeth. The sampling areas for LA-ICP-MS were chosen because they included pre- and post-natal regions of enamel and dentine as well as the neonatal line. No predetermination of sample size was done, and samples were chosen on availability of material and suitability for consumptive sampling.
Data collection	Growth increments in the enamel and dentine were manually traced and counted from high-resolution digital photomontages produced using the automated "photomerge" feature of Adobe Photoshop CC 2021. Traces and counts were performed by GFF. LA-ICP-MS data was collected automatically, using an ATLEX-I-LR Analyte Excite 193nm ArF excimer coupled to an Attom ICPMS, Nu Instrument operated by LEP at the University of Edinburgh, and a Laurin Technic S155 2-volume ablation cell featuring a 193 nm ASI Resolution ArF excimer laser coupled to an Agilent 8900 Triple Quadrupole ICP-MS operated by JTS and MD at the University of St. Andrews.
Timing and spatial scale	Histological data was collected between June 2020 and April 2022. LA-ICP-MS data was collected between June 30, 2021, and February 15, 2022. Sampling was not periodic or organized into cohorts.
Data exclusions	Pilot LA-ICP-MS transects were collected to evaluate the suitability of the material for more comprehensive analysis. Pilot transects were not rigorously controlled with respect to orientation, direction, or spot size, and therefore do not reflect biological signals. For these reasons, these transects were not considered in our final analyses.
Reproducibility	Replication is not applicable to the study because there were no experimental groups.
Randomization	Randomization was not applied because there were no experimental groups.
Blinding	Blinding was not used because there were no experimental groups.

Did the study involve field work? ☐ Yes ☒ No

Reporting for specific materials, systems and methods

We require information from authors about some types of materials, experimental systems and methods used in many studies. Here, indicate whether each material, system or method listed is relevant to your study. If you are not sure if a list item applies to your research, read the appropriate section before selecting a response.

Materials & experimental systems

n/a	Involved in the study
☒	☐ Antibodies
☒	☐ Eukaryotic cell lines
☐	☒ Palaeontology and archaeology
☒	☐ Animals and other organisms
☒	☐ Human research participants
☒	☐ Clinical data
☒	☐ Dual use research of concern

Methods

n/a	Involved in the study
☒	☐ ChIP-seq
☒	☐ Flow cytometry
☒	☐ MRI-based neuroimaging

Palaeontology and Archaeology

Specimen provenance	Nacimiento Formation, San Juan Basin, New Mexico, USA. Specimens collected under US BLM Paleontological Use Permit # NMMNH 8270-RS-8C. Permission for destructive analysis was provided by the New Mexico Museum of Natural History and Science February 25, 2022.
Specimen deposition	New Mexico Museum of Natural History
Dating methods	No new dates are provided

☒ Tick this box to confirm that the raw and calibrated dates are available in the paper or in Supplementary Information.

Ethics oversight	Fieldwork permits were granted by the Bureau of Land Management of the United States of America (US BLM Paleontological Use Permit # NMMNH 8270-RS-8C). No other ethical approval or guidance required for the study.

Note that full information on the approval of the study protocol must also be provided in the manuscript.